

Data-Based Distillation: Teaching What You Should Teach

Shitong Shao¹, Huanran Chen¹, Zhen Huang², Linrui Gong³, Shuai Wang⁴ and Xinxiao Wu¹

¹School of Computer Science, Beijing Institute of Technology, Beijing, China

²University of Science and Technology of China, Hefei, China

³Hunan University, Hunan, China

⁴Tsinghua University, Beijing, China

1090784053sst@gmail.com, huanranchen@bit.edu.cn, zhenhuang@mail.ustc.edu.cn, hunan
s-wang20@mails.tsinghua.edu.cn, wuxinxiao@bit.edu.cn

Abstract

In real teaching scenarios, an excellent teacher always teaches what he (or she) is good at but the student is not. This method gives the student the best assistance in making up for his (or her) weaknesses and becoming a good one overall. Enlightened by this, we introduce the approach to the knowledge distillation framework and propose a data-based distillation method named “Teaching what you Should Teach (TST)”. To be specific, TST contains a neural network-based data augmentation module with the priori bias, which can assist in finding what the teacher is good at while the student are not by learning magnitudes and probabilities to generate suitable samples. By training the data augmentation module and the generalized distillation paradigm in turn, a student model that has excellent generalization ability can be created. To verify the effectiveness of TST, we conducted extensive comparative experiments on object recognition (CIFAR-100 and ImageNet-1k), detection (MS-COCO), and segmentation (Cityscapes) tasks. As experimentally demonstrated, TST achieves state-of-the-art performance on almost all teacher-student pairs. Furthermore, we conduct intriguing studies of TST, including how to solve the performance degradation caused by the stronger teacher and what magnitudes and probabilities are needed for the distillation framework.

1 Introduction

In recent years, deep neural networks have been widely applied in many fields [55; 51; 42], such as computer vision [55; 51; 42], natural language processing [58; 16; 2], reinforcement learning [37; 7; 41] and speech signal processing [40]. However, the improving performance of the deep learning model is always achieved by the increasing size of the model, which makes it inconvenient for us to train or deploy our models further [21; 17]. To alleviate this problem, researchers have developed a series of model compression algorithms, such as parameter pruning [19], quantization [52], and knowledge distillation [23].

Inspired by the teaching process in the human world, knowledge distillation was proposed by [23], which aims to improve the target model or so-called student model, by teaching this model with a better teacher model instead of only ground truth labels. There are two mainstream approaches to distilling knowledge from the teacher to the student. One is the logit-based distillation, which means that the student is supervised not only by the ground truth labels but also the output of the teacher. The second is the feature-based distillation, which not only aligns the output of the student and the teacher, but also aligns the activation map in some layers. These two methods have developed rapidly in the past decade, helping us get efficient and effective models that are not possible to get from traditional supervised learning [48; 1; 39; 38; 57; 8]. However, These two research directions entered a bottleneck in recent years, making it hard for researchers to devise more methods that get significant improvements.

In this work, we rethink the knowledge distillation algorithm from a new perspective and propose a new data-based distillation method. In a real-world teaching scenario, the teaching should be considered not only from the mode but also the content. Compared with studying the problems that the teacher is not good at, it is more efficient and helpful for the student to study the problems that the teacher is skilled at. The research of logit-based knowledge distillation and feature-based knowledge distillation can be seen as finding new teaching styles and teaching ways. Our goal in this work is to find what the teacher is good at and let the teacher only teach the knowledge that it should teach to boost the performance and effectiveness of the student.

More specifically, we propose a novel data-based distillation method, named “Teaching what you Should Teach (TST),” which can improve the student’s generalization ability by generating a series of new samples that the teacher excels at but the student does not. We design a mechanism that contains a data augmentation encoder that aims to generate augmented samples that the teacher is good at while the student is not good at; then, the teacher utilizes these augmented samples to guide the student. Note that this encoder is differentiable and stable, the safety and diversity of generated samples can be ensured since it introduces manual data augmentations (e.g., Translate, Rotate, and Solarize) and employs the microscopic property of meta-encoders. In addi-

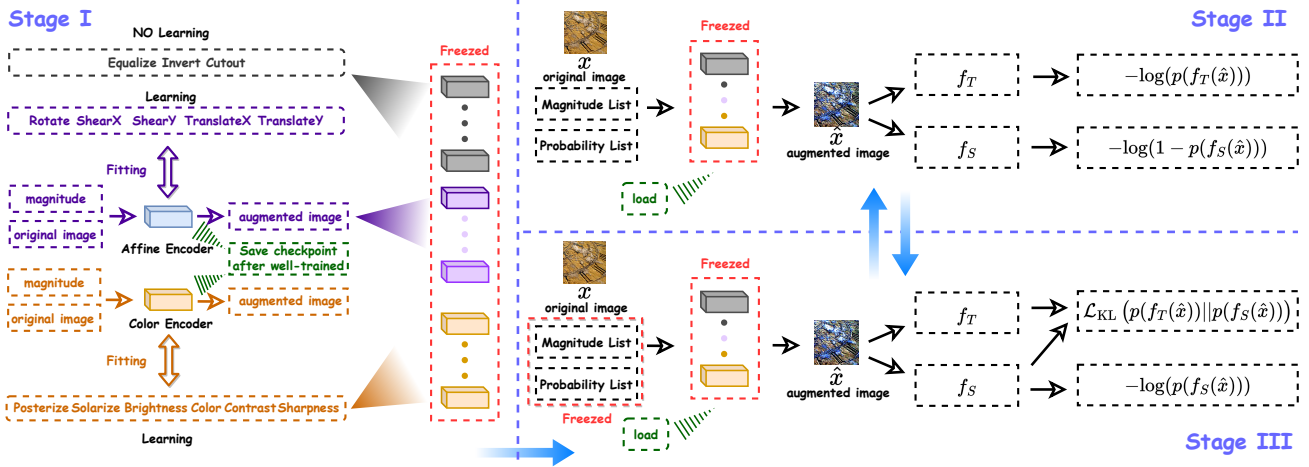


Figure 1: The overall framework of TST. In Stage I, we introduce a priori bias about data augmentation into the neural network-based data augmentation module. Then, we switch between updating magnitudes and probabilities in Stage II and θ_S in Stage III to make up for as many of the weaknesses of the student as possible.

tion, we assume that it is easy for TST to generate samples that meet its requirements, which is difficult for the student to learn, thus, we make the number of training iterations of the encoder much smaller than that of the student to ensure the distilled students have the most robust performance improvement.

As demonstrated in Sec. 4, our proposed TST is experimented with on relevant benchmark datasets, including image classification (CIFAR-100 [28] and ImageNet-1k [44]), object detection (MS-COCO [31]), and semantic segmentation (Cityscapes [11]). It achieves state-of-the-art performance in all quantitative comparison experiments with fair comparison, indicating that data-based distillation is feasible and needs more scholarly attention. Moreover, we conducted a chain of ablation studies and discovered that TST is effective and the assumptions set out above are correct.

Our contribution can be summarized as follows:

- We rethink the knowledge distillation methods from a new perspective, which not only summarizes the previous works but also helps us propose a new idea, improving knowledge distillation by teaching methods as well as using more desirable data.
- In order to achieve our goal, we devise a mechanism to help us judge whether the data is suitable for distillation. We introduce a differentiable and stable data augmentation encoder to generate more data like that. By fitting the meta-encoders to the priori manual data augmentation, we ensure the interpretability of the TST and the stability of the data augmentation encoder.
- We did plenty of ablation studies to verify the effectiveness of TST. Besides, we discuss and analyze the phenomenon, i.e., the degradation of distillation performance brought by the stronger teacher in the framework of TST, and then propose a solution. We visualize the characteristic information of the data augmentation encoder learned by TST and discover some patterns in it.

2 Related Work

Data Generation Encoder. A data generation encoder is designed to encode noisy signals or old images to create new ones. Due to the various task types, the newly generated images usually have different characteristics (e.g., high resolution [4; 14], different styles [50], different semantics [61]). Some popular data generation encoders, including VAE [27], GAN [20], and diffusion models [24]. These models cannot be used for data-based distillation because their input samples are noisy signals and their training costs are prohibitively expensive. Therefore, we focus on lightweight data encoding modules, including style-complement module [50], differentiable data augmentation module [29], and neural network-based data augmentation module [46], in which both input and output are images. However, these data generators encoders cannot be directly applied in our framework. The style-complement module is susceptible to training process which can leads to training failure because it lacks the priori augmentation bias. And the training paradigm of the differentiable data augmentation module is overly complex. For the neural network-based data augmentation module, it does not have diversity in data transformation, which is not desirable to boost the model performance. To solve these issues, we add the priori bias to the neural network-based data augmentation module and then freeze it in standard training. This ensures that the new data encoder is interpretable and diverse.

Data-Based Distillation. In the field of knowledge distillation, past researchers have only focused on feature-based as well as logit-based distillation methods in the generic distillation framework. However, these works ignored the data level, which is the first guarantee that a model can obtain good generalization ability. Data-free knowledge distillation, as a subfield of knowledge distillation, can be regarded as an application scenario of data-based distillation framework [54; 18]. Researchers apply this framework to extract the teacher’s implicit knowledge for the purpose of synthesizing plausi-

ble new samples, which are then used to facilitate knowledge transfer. Data-free distillation approaches are typically performed by reducing noise and imposing constraints to ensure that more natural-looking synthetic images are generated. In generic knowledge distillation, training data is always sufficient, which means that we do not have to utilize gaussian noise to synthesize images. In this case, data-based distillation has not been investigated in the generic distillation framework. To fill this gap, we turn to focus on designing a data-based distillation method and use a data augmentation encoder to obtain new samples from the original samples that can be recognized by the teacher but not by the student.

3 Teach What You Should Teach

In this section, we first introduce the total framework of our Data-Based Distillation, i.e. TST. Then, we describe the details of neural network-based data augmentation module.

3.1 Total Framework

TST first introduces the reasonable priori bias into the neural network-based data augmentation module and then adversarially alternates Stage II and Stage III to obtain an excellent student. In order to state TST more logically, we start with an introduction to a general knowledge distillation framework, which can be interpreted as follows: given a teacher f_T with parameter θ_T and a student f_S with parameter θ_S , when a training set \mathcal{X} is utilized for training, we can sample the mini-batch $\{x^k\}_{k=1}^B$ (B denotes to the batch size) from it and get the student output $\{f_S(x^k)\}_{k=1}^B$ and the teacher output $\{f_T(x^k)\}_{k=1}^B$ by forward propagation. Let us define the normalized exponential function p , i.e., softmax, to calculate the probability distribution of the model output. The goal of knowledge distillation is to minimize the cross-entropy loss \mathcal{L}_{CE} between $\{p(f_S(x^k))\}_{k=1}^B$ and the ground truth label $\{y^k\}_{k=1}^B$, and the Kullback-Leibler divergence \mathcal{L}_{KL} between $\{p(f_T(x^k))\}_{k=1}^B$ and $\{p(f_S(x^k))\}_{k=1}^B$. Thus, the total loss function \mathcal{L}_{total} can be formulated as:

$$\mathcal{L}_{total} = \frac{1}{B} \sum_{k=1}^B w_{ce} \mathcal{L}_{CE} \left(p(f_S(x^k)), y^k \right) + w_{kl} \mathcal{L}_{KL} \left(p(f_T(x^k)) || p(f_S(x^k)) \right), \quad (1)$$

where w_{ce} and w_{kl} are balanced weights. Eq. 1 is equivalent to the paradigm in Stage III of Fig. 1 that discards the neural network-based data augmentation module.

The goal of TST is to assist the student in overcoming its deficiencies in the generic distillation paradigm by discovering a new set of samples that the teacher excels at but the student does not through the data encoder. We denote the data encoder f_{DE} contains a data augmentation meta-encoder set $\{f_E^i\}_{i=1}^N$ with a parameter set $\{\theta_E^i, \theta_p^i\}_{i=1}^N \cup \{\theta_m^i\}_{i=1}^{N-N_{nl}}$, where N and N_{nl} refer to the total number of all sub-policies and the total number of sub-policies without magnitudes. All sub-policies (e.g., Equalize, Rotate, Posterize) are displayed in Stage I of Fig. 1. Note that each f_E has the frozen parameter θ_E containing the priori bias, and its other parameters,

i.e., the magnitude¹ θ_m and the probability θ_p , are learnable in Stage II. Therefore, as illustrated in Fig. 1, we can denote the loss function of TST in Stage II as:

$$\mathcal{L}_{TST} = \frac{1}{B} \sum_{k=1}^B \alpha \mathcal{L}_{CE} \left(p(f_T(\hat{x}^k)), y^k \right) + \beta \mathcal{L}_{CE} \left(1 - p(f_S(\hat{x}^k)), y^k \right), \quad (2)$$

where \hat{x} , α and β denotes the augmented sample obtained from the original sample after f_{DE} , a balanced weight of $\mathcal{L}_{CE} \left(p(f_T(\hat{x}^k)), y^k \right)$ and a balanced weight of $\mathcal{L}_{CE} \left(1 - p(f_S(\hat{x}^k)), y^k \right)$, respectively. Specific details about f_{DE} will be presented in Sec. 3.2. The optimization objective of Stage II $\min_{\{\theta_m^i, \theta_p^i\}_{i=1}^N} \mathcal{L}_{TST}$ is to let the student misclassify but

let the teacher correctly classify so that the teacher can transfer the most helpful knowledge to students. To better find new samples that students cannot classify correctly, we use $\mathcal{L}_{CE} \left(1 - p(f_S(\hat{x}^k)), y^k \right)$ instead of $-\mathcal{L}_{CE} \left(p(f_S(\hat{x}^k)), y^k \right)$ to avoid non-convex optimization, and the proof can be found in Appendix D. Moreover, the parameters $\{\theta_E^i\}_{i=1}^N$ are frozen because they contain the priori bias in favor of distillation, which is imported in Stage I of Fig. 1. As demonstrated later in Sec. 4.2, distillation can easily fail if $\{\theta_E^i\}_{i=1}^N$ is not frozen due to the instability of the data augmentation module.

During standard distillation training, Stage II and Stage III alternate. Specifically, TST first employs Stage II to find new samples suitable for distillation, and then utilizes Stage III to improve the student's generalization ability. Inspired by [3], we claim that it is easy to search augmented samples in Stage II that match what the teacher is good at but the student is not, while it is difficult for the student to absorb knowledge contained in the augmented samples in Stage III. Therefore, the number of iterations $n_{encoder}$ of Stage II will be much smaller than the number of iterations $n_{student}$ of Stage III. Sec. 4.2 illustrates that the student trained by TST will have better performance when $n_{encoder} \ll n_{student}$.

As illustrated on the left in Fig. 1, Stage I is applied to introduce the augmented priori bias into f_{DE} . For simplicity, we consider each meta-encoder f_E in the set $\{f_E^i\}_{i=1}^N$ as a black box in this paragraph. In stage I, since Equalize, Invert and Cutout do not have the property of magnitude, they do not need to be fitted and can be called directly in Stage II and Stage III. Of course, their probabilities are learnable and will still be optimized in Stage II. Then, we categorize a series of single data augmentations as follows: (a) magnitude-unlearnable transformations, including Equalize, Invert, and Cutout; (b) learnable affine transformations, including Rotate, ShearX, ShearY, TranslateX, and TranslateY; (c) learnable color transformations, including Posterize, Solarize, Brightness, Color, Contrast, and Sharpness [12; 13]. For the learnable affine transformations and color transformations, we apply Spatial Transformer Network [26] and Color Network for fitting, respectively. Since both types (a) and (b) are fitted in the same way, we define a set of the man-

¹Magnitudes indicate the strength of the sub-policies transition. Some sub-policies do not have this variable, such as Cutout, Equalize, and Invert. These details will be introduced later.

Table 1: **Results on CIFAR-100 test set.** Same and Different in the first row refer to whether the model architecture is the same for teachers and students. All results are the average over 3 trials.

Architectures		Same						Different		
Distillation Type	Teacher	ResNet110	ResNet110	WRN-40-2	WRN-40-2	ResNet32×4	VGG13	WRN40-2	ResNet32×4	VGG13
	Student	74.31	74.31	75.61	75.61	79.42	74.64	75.61	79.42	75.61
Feature-based	FitNet	68.99	71.06	72.24	73.58	73.50	71.02	73.73	73.59	64.14
	ATKD	70.22	70.55	72.77	74.08	73.44	71.43	73.32	72.73	59.40
	SPKD	70.04	72.69	72.43	73.83	72.94	72.68	74.52	73.48	66.30
	CCKD	69.48	71.48	72.21	73.56	72.97	70.71	71.38	71.14	64.86
	RKD	69.25	71.82	72.22	73.35	71.90	71.48	72.21	72.28	64.52
	VID	70.16	70.38	73.30	74.11	73.09	71.23	73.61	73.38	65.56
	CRD	71.46	73.48	74.14	75.48	75.51	73.94	76.05	75.11	69.73
	OFD	-	73.23	74.33	75.24	74.95	73.95	75.85	75.98	69.48
	ReviewKD	-	71.89	75.09	76.12	75.63	74.84	77.14	77.45	70.37
	KD	70.67	73.08	73.54	74.92	73.33	72.98	74.83	74.07	67.37
Logit-based	DKD	-	74.11	74.81	76.24	76.32	74.68	76.70	76.45	69.71
	DIST	69.94	73.55	74.42	75.29	75.79	73.74	75.23	75.23	68.48
Data-based	Ours	72.44	75.04	75.32	76.75	76.72	75.03	77.38	76.71	70.82

Table 2: **Results on ImageNet validation set.** L-B: Logit-Based Distillation. F-B: Feature-Based Distillation. D-B: Data-Based Distillation. We use ResNet-34 and ResNet-50 released by Torchvision [36] and Swin-Large released by [34] as our teacher’s pre-training weight.

Architecture		Accuracy		L-B	F-B	F-B	F-B	F-B	F-B	L-B	L-B	D-B	
Teacher	Student	Teacher	Student	KD [23]	OFD	RKD [38]	CRD [47]	SRRL	ReviewKD [6]	DKD	DIST [25]	Ours	
ResNet-34	ResNet-18	Top-1	73.31	69.76	70.66	71.08	70.34	71.17	71.73	71.61	71.70	72.07	72.22
		Top-5	91.42	89.08	89.88	90.07	90.37	90.13	90.60	90.51	90.41	90.42	90.68
ResNet-50	MobileNet-V1	Top-1	76.16	70.13	70.68	71.25	-	71.37	72.49	72.56	72.05	73.24	72.31
		Top-5	92.86	89.49	90.30	90.34	-	90.41	90.92	91.00	91.05	91.12	90.70
Swin-Large	Swin-Tiny	Top-1	86.30	81.30	81.50	-	81.20	-	81.50	-	-	82.26	82.21

ual data-augmentation mappings $\{f_A^i\}_{i=1}^{N-N_{\text{nl}}}$ that includes all single data augmentations with magnitude. For each matched pair f_A and f_E in $\{f_A^i\}_{i=1}^{N-N_{\text{nl}}}$ and $\{f_E^i\}_{i=1}^{N-N_{\text{nl}}}$, we will optimize Mean Square Error function (\mathcal{L}_{MSE}) by n_{fitting} iterations. The loss function in Stage I can be formulated as:

$$\mathcal{L}_{\text{encoder}} = \frac{1}{B} \sum_{k=1}^B \|f_A(x^k, m_r) - f_E(x^k, m_r)\|_2, \quad (3)$$

where m_r refers to a random value $\sim \mathcal{U}(0, 1)$. In our experiments, $\mathcal{L}_{\text{encoder}}$ will be optimized to a very small error bound after n_{encoder} iterations. This guarantees that all meta-encoders are well-trained.

Particularly, since the teacher was trained on the original training set, we argue that it must be suitable for distillation. As a result, the samples applied in training are composed of the original and augmented samples. Finally, more detailed algorithmic procedure can be found in Appendix C.

3.2 Network-Based Data Augmentation Module

We will describe the whole process of how x goes through f_{DE} and finally becomes \hat{x} in this sub-section. We first describe how f_{DE} calls $\{f_E^i\}_{i=1}^N$ to accomplish the combination of various sub-generated samples, and then we present the details of Spatial Transformer Network and Color Network.

After normalizing $\{\theta_m^i\}_{i=1}^{N-N_{\text{nl}}}$ and $\{\theta_p^i\}_{i=1}^N$ to $[0 \sim 1]$ by applying the sigmoid activation function, we employ the Relaxed Bernoulli Distribution to sample new magnitudes and probabilities for solving the non-differentiable problem [30;

29]. The process can be formulated as:

$$\begin{aligned} \text{RBD}(p) &= \text{sigmoid}((\log(p) + L)/\tau), L \sim \text{Logistic}(0, 1), \\ \{\theta_m^i\}_{i=1}^{N-N_{\text{nl}}} &= \left\{ \text{RBD} \left(\text{sigmoid} \left(\theta_m^i \right) \right) \right\}_{i=1}^{N-N_{\text{nl}}}, \\ \{\theta_p^i\}_{i=1}^N &= \left\{ \text{RBD} \left(\text{sigmoid} \left(\theta_p^i \right) \right) \right\}_{i=1}^N, \end{aligned} \quad (4)$$

where *Logistic* and τ stand for the logistic distribution and the temperature, respectively. In our all experiments, τ is set as 0.05. Then, we randomly select N_A non-repeating numbers $\{Z^i\}_{i=1}^{N_A}$ from $\{i\}_{i=1}^N$. N_A can be interpreted as the encoding strength of f_{DE} , i.e., a larger N_A means that the model is more difficult to identify the augmented samples. N_A is set as 4 by default in our experiments. As denoted in Eq. 5, we obtain $\{x_E^i\}_{i=1}^{N_A}$ from x through all meta-encoders and get the final \hat{x} by simple sum.

$$\begin{aligned} x_E^i &= \begin{cases} \theta_p^{Z^i} \odot f_E(x, \theta_m^i) - \theta_p^{Z^i} \odot x, & Z^i \leq N_{\text{nl}} \\ \theta_p^{Z^i} \odot f_E(x) - \theta_p^{Z^i} \odot x, & Z^i > N_{\text{nl}} \end{cases} \\ \hat{x} &= x + \sum_{i=1}^{N_A} x_E^i, \end{aligned} \quad (5)$$

where \odot denotes the element-wise product. For object detection tasks, the summation of affine transformation results in Eq. 5 can easily lead to a single target object becoming multiple target objects. Therefore, we use a separate algorithm for this special task, which is explained in Appendix D.

Spatial Transformer Network f_{STN} and Color Network f_{CN} are two different neural network-based meta-encoders. Each has parameters θ_E to store the priori bias learned from Stage I. However, f_{STN} and f_{CN} employ different ways to complete

Table 3: **Results on the COCO validation set (T→S refers to the distillation from T to S).** Here, the content in brackets to the right of “Ours” refers to the methods applied in the distillation process. In addition, CM RCNN-X101 stands for Cascade Mask RCNN-X101.

T→S Type Method	CM RCNN-X101→Faster RCNN-R50						RetinaNet-X101→RetinaNet-R50						T→S Type Method	FCOS-R101→FCOS-R50						
	Two-stage detectors						One-stage detectors							Anchor-free detectors						
	AP	AP ₅₀	AP ₇₅	AP _S	AP _M	AP _L	AP	AP ₅₀	AP ₇₅	AP _S	AP _M	AP _L		AP	AP ₅₀	AP ₇₅	AP _S	AP _M	AP _L	
Teacher	45.6	64.1	49.7	26.2	49.6	60.0	41.0	60.9	44.0	23.9	45.2	54.0	KD [23]	40.8	60.0	44.0	24.2	44.3	52.4	
Student	38.4	59.0	42.0	21.5	42.1	50.3	37.4	56.7	39.6	20.0	40.7	49.7	KD [23]	38.5	57.7	41.0	21.9	42.8	48.6	
COFD [22]	39.7	61.2	43.0	23.2	43.3	51.7	37.2	56.5	39.3	20.4	40.4	49.5	Fitnet [43]	39.9	58.4	42.8	23.6	44.0	51.1	
FKD [56]	38.9	60.1	42.6	21.8	42.7	50.7	37.8	58.3	41.1	21.6	41.2	48.3	GID [15]	39.9	58.6	43.1	23.1	43.4	52.2	
DIST [25]	41.5	62.2	45.1	23.5	45.0	55.3	39.6	58.8	42.1	22.7	43.3	52.5	FRS [60]	42.0	60.4	45.5	25.6	45.8	54.2	
DIST+mimic [25]	40.4	61.7	43.8	23.9	44.6	52.6	39.8	59.5	42.5	22.0	43.7	53.0	FGD [53]	40.9	60.3	43.6	25.7	45.2	51.2	
Ours (KD)	41.8	62.4	45.6	23.4	46.1	55.0	40.1	59.4	43.0	23.2	44.0	53.6	Ours (KD)	42.1	-	-	27.0	46.0	54.6	
Ours (KD+mimic)	40.5	62.4	44.1	24.0	44.6	52.1	39.9	59.6	42.8	23.3	43.8	53.3	Ours (KD+mimic)	40.1	58.3	43.2	23.9	44.1	51.6	
Ours (KD+mimic)	42.2	63.4	46.1	24.1	46.5	55.6	40.5	60.0	43.4	23.9	44.5	54.4	Ours (KD+mimic)	41.0	60.0	44.3	24.9	45.0	51.8	

Table 4: **Results on the Cityscapes validation set.** *: The experiments are performed based on mmrazor [10].

Method	mIoU (%)	Method	mIoU (%)
T: PSPNet-R101	78.55	S: PSPNet-R18	70.09
SKDD [33]	74.08	SKDS [32]	72.70
IFVD [49]	74.54	CWD [45]*	75.54
DIST [25]	75.74	Ours*	76.55

the calculation. As shown in Eq. 6, when x and magnitude m are fed into f_{STN} , θ_E (can be considered as a vector) is first concatenated with m to form a new vector $\hat{\theta}_E$, and then passes through a fully connected layer $\mathcal{FC} := \mathbb{R}^{\text{len}(\theta_E)+1} \rightarrow \mathbb{R}^6$ to obtain the matrix $A \in \mathbb{R}^{2 \times 3}$.

$$f_{\text{STN}}(x, m) = \text{Affine}(A, x), \quad \text{where } A = \text{reshape}(\mathcal{FC}([\theta_E, m])). \quad (6)$$

For f_{CN} , its forward propagation is composed of convolution and color transformation. So, θ_E not only has a vector $\theta_{E,V}$ but also a convolution weight $\theta_{E,C}$ to record the priori bias. When x and m are fed into f_{CN} , $\theta_{E,V}$ and m concatenate a new vector $\hat{\theta}_{E,V}$, and we let it through a fully connected layer $\mathcal{FC} := \mathbb{R}^{\text{len}(\theta_{E,V})+1} \rightarrow \mathbb{R}^2$ to obtain the scale and shift parameters, i.e., θ_{scale} and θ_{shift} . After that, the output of f_{CN} can be denoted as:

$$f_{\text{CN}}(x, m) = \mathcal{C}(x \odot (0.5 + \text{sigmoid}(\theta_{\text{scale}})) + \text{sigmoid}(\theta_{\text{shift}}) - 0.5), \quad (7)$$

where \mathcal{C} refers to the convolutional layer. In particular, in our experiments, we perform RBD on A , θ_{shift} and θ_{scale} additionally to guarantee the diversity of data augmentation to prevent $\{\theta_m^i\}_{i=1}^{N-N_{\text{nl}}}$ and $\{\theta_p^i\}_{i=1}^N$ from converging to a locally optimal solution.

4 Experiment

We conduct comparison experiments on three major tasks: image classification, object detection, and semantic segmentation. The image classification datasets include CIFAR-100 and ImageNet-1k; the target detection dataset includes MS-COCO; the semantic segmentation dataset includes Cityscapes. More details about these datasets can be found in Appendix A. Besides, all the experiment results on CIFAR-100 are the average over five trials, while the related experiment results on other datasets are the average over three trials. We apply batch size 128 and initial learning rate 0.1

on CIFAR-100. And we follow the settings in [25] for the ResNet34-ResNet18 pair and the ResNet50-MobileNet pair on ImageNet-1k. The settings of other classification, detection and segmentation tasks can be found in Appendix B. Note that all the **bolded values** in tables refer to the optimal results.

4.1 Comparison Experiment with SOTA Methods

Classification on CIFAR-100. We compare many state-of-the-art feature-based as well as logit-based distillation algorithms on 9 student-teacher pairs. For these teacher-student pairs, the teacher and student of 6 pairs have the same structure, and the teacher and student of the other 3 pairs have different architecture. The experimental results are presented in Tab. 1. Obviously, we can find that TST, as the only data-based distillation approach, outperforms all other algorithms on 8 student-teacher pairs except for ResNet32×4-ShuffleNet-V1. Especially on 3 teacher-student pairs, including ResNet110-ResNet20, ResNet110-ResNet32 and VGG13-VGG8, we surpass the latest state-of-the-art methods by almost more than one percent. Besides, in order to more fully demonstrate the excellent performance of the TST, we conduct simulations of few-shot scenarios on CIFAR-100. Here, we follow the training settings in [47] and randomly discard 25%, 50%, and 75% samples for training. As the experimental results shown in Tab. 5, TST also performs well in this few-shot scenario.

Table 5: Top-1 accuracy (%) comparison of the few-shot scenario on CIFAR-100. Here, all teacher-student pairs are ResNet56-ResNet20 pairs.

Percentage	KD	CRD	Ours
25%	65.15	65.80	66.28
50%	68.61	69.91	70.22
75%	70.34	70.68	71.80

Classification on ImageNet-1k. We further demonstrate whether TST can work robustly on ImageNet and conduct experiments with two different architecture pairs, including Conv-Conv and ViT-ViT pairs. For Conv-Conv pair, we consider two teacher-student pairs: ResNet34-ResNet18 and ResNet50-MobileNet-V1 pairs, and apply the same hyper-parameter settings to examine the effectiveness of the TST. The results are illustrated in Tab. 2. We can find that TST beats all state-of-the-art methods in ResNet34-ResNet18 pair but is slightly inferior to SRRL, ReviewKD and DIST in ResNet50-MobileNet-V1 pair. The reason that TST does not

Table 6: T-S pair: Teacher-Student pair. Top-1 accuracy (%) comparison of whether the neural network-based data augmentation module is learnable or not on CIFAR-100.

Teacher	Student	Learnable	N_A		
			2	4	6
WRN-40-2	WRN-16-2	Yes	76.75	76.58	76.55
		No	76.41	76.05	75.66
ResNet110	ResNet20	Yes	72.34	72.44	72.43
		No	71.86	71.74	71.80

perform excellently on ResNet50-MobileNet-V1 pair is that the teacher is stronger, which causes the teacher overconfident in discriminating on the original and generating augmented samples. In our discussion, we consider this phenomenon in isolation and give two solutions for mitigating poor student performance under TST finishing with the stronger teacher. In particular, this is not a defect of TST, but rather due to the fact that \mathcal{L}_{KL} is not adapted to the distillation process with the stronger teacher. In fact, there are many approaches, including DIST [25] and DKD [57], that have been proposed to alleviate the gap between the teacher and student. For the VIT-VIT pair, we regard Swin Transformer [34], which is widely known and applied by researchers, as the model architecture in distillation. We treat Swin Transformer Tiny (Swin-Tiny) as the student and Swin-Transformer Large (Swin-Large) as the teacher. The experimental results are presented in Tab. 2, where TST surpasses all methods except DIST, proving that TST is applicable to VIT-based architectures.

Detection on MS-COCO. Comparison experiments are run on three kinds of different detectors, i.e., *two-Stage detectors*, *one-stage detectors*, *anchor-free detectors*. In particular, TST introduces additional losses on Stage II that drove the student box regression to be inaccurate and the teacher box regression to be accurate. As shown in Tab. 3, TST breaks the vanilla KD bottleneck by locating augmented samples that are conducive to distillation. Due to the additional loss on box regression in Stage II and the fact that the detection task depends more on the network’s ability to produce good features, we trust that aligning the student and teacher feature maps will improve the performance of TST. Thus, we follow [25] by adding auxiliary loss mimic, i.e., translating the student feature map to the teacher feature map by a convolution layer and supervising them utilizing \mathcal{L}_{MSE} , to the detection distillation task. Ultimately, we can conclude from Tab. 3 that TST based on the vanilla KD and mimic achieves the best performance on Cascade RCNN-X101-Cascade RCNN-R50 and RetinaNet-X101-RetinaNet-R50 pairs.

Segmentation on Cityscapes. As shown in Tab. 4, we conduct comparative experiments of semantic segmentation on PSPNet-R101-PSPNet-R18 pair [59]. As a result, TST outperforms all comparative methods and improves mIoU by nearly one percent compared to the latest state-of-the-art method, DIST.

4.2 Ablation Study

We conduct ablation studies in three aspects: **(a)** the effect of whether the TST executes Stage II on the student perfor-

Table 7: Top-1 accuracy (%) comparison on CIFAR-100. Here, we performed ablation experiments on n_{encoder} . N_A for all experiments in this table is set as 4.

Teacher	Student	n_{encoder}			
		$0 \cdot \frac{ \mathcal{X} }{B}$	$1 \cdot \frac{ \mathcal{X} }{B}$	$15 \cdot \frac{ \mathcal{X} }{B}$	$30 \cdot \frac{ \mathcal{X} }{B}$
WRN-40-2	WRN-16-2	76.05	76.72	76.53	76.58
		71.74	72.46	72.41	72.44

Table 8: Top-1 accuracy (%) comparison for different data encoders on CIFAR-100. Here, + and * stand for not freezing all the parameters in $\{f_E^i\}_{i=1}^N$ and not introducing bias of a priori data augmentation into $\{f_E^i\}_{i=1}^N$, respectively. The results “NAN” represents the gradient explosion. Besides, N_A and n_{encoder} for all experiments in this table is set as 4 and $30 \cdot \frac{|\mathcal{X}|}{B}$, respectively.

Teacher	Student	Mode			
		Attack	Ours ⁺	Ours ⁺⁺	Ours
WRN-40-2	WRN-16-2	74.76	66.01	NAN	76.58
		71.15	52.91	NAN	72.44

mance; **(b)** the different iteration number of Stage II; **(c)** the impact of varying data encoders on TST.

As illustrated in Tab. 6, no matter what kind of teacher-student pairs or whatever value of N_A , the augmented sample search strategy of TST, i.e., Stage II, is always beneficial for distillation.

In addition, we suppose that TST may easily find augmented samples that the student is not good at, but it is difficult for the student to absorb the corresponding knowledge fully. Based on this conjecture, TST should perform best in the case that $n_{\text{encoder}} \ll n_{\text{student}}$. The experimental results in Tab. 7 prove our assumption. Note that $\frac{|\mathcal{X}|}{B}$ actually refers to the iteration number within an epoch.

At last, we show the impact of different types of data encoders on the performance of TST in Tab. 8 and analyze it. One of the data encoders, Attack, denotes the direct manipulation of samples in a form similar to PGD [35], which means that TST must let Stage II and Stage III iterate once each in turn and repeat the process. Based on the findings in Tab. 8, we can indicate that it is an extremely sensible choice to introduce the augmented priori bias into the data encoder and to freeze the parameters associated with the bias during distillation process.

5 Discussion

How to alleviate the gap between the teacher and student? To analyze this situation, we train two stronger teachers, including WRN-40-4 and WRN-28-10, achieve 80.7% and 82.0% Top-1 accuracy on the test set of CIFAR-100, respectively. Then, we employ these two teachers for a more in-depth exploration. As illustrated in Tab. 9, when w_{ce} , w_{kl} , α and β take default values (i.e., 1, 1, 1 and 1), stronger teachers (i.e., WRN-40-4 and WRN-28-10) usually achieve worse performance compared to WRN-40-2. To analyze this phenomenon, we show in Fig. 2 that the teacher’s response to the ground truth label, i.e., the probabilities of correctly discriminating samples. Specifically, in each epoch of Stage III, we

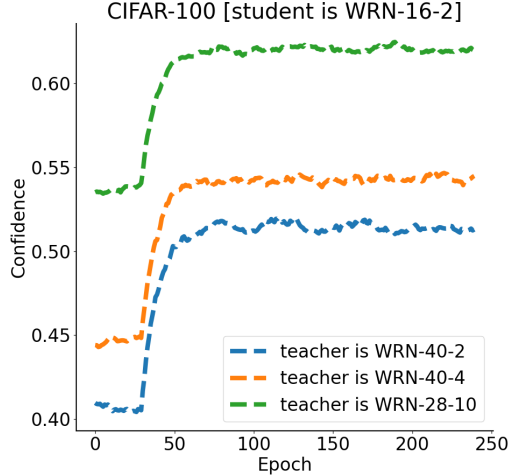


Figure 2: The probability of different-size teachers predicting samples correctly with epochs. Here, this figure is intended to supplement the discussion section.

Table 9: Top-1 accuracy (%) comparison on CIFAR-100. Analytical experiments of w_{ce} , w_{kl} , α and β hyperparameters. Here, all students are WRN-16-2.

Hyperparameters	Teacher				
	WRN-40-4	WRN-28-10	w_{ce}	w_{kl}	
α	β				
1.0	1.0	75.93	75.79	1.00	1.00
1.0	1.0	76.13	76.04	0.95	1.05
1.0	0.85	76.35	76.18	0.85	1.15
1.0	0.75	76.42	76.34	0.75	1.25
1.0	0.5	76.45	75.80	0.5	1.5
1.0	0.25	76.19	75.81	0.25	1.75
0.8	1.2	76.32	75.89	1.2	1.00
0.6	1.4	76.37	75.96	1.4	1.00
0.4	1.6	76.47	76.02	1.6	1.00
0.2	1.8	76.29	76.17	1.8	1.00

get the teacher’s responses to the correct category corresponding to all training samples, and plot the expectation of the responses. This indicates that the stronger the teacher is, the closer its response is to one-hot encoding and the less “dark knowledge” attached to the logit. Consequently, the performance degradation of students caused by stronger teachers can be mitigated by making the teacher logit not too close to one-hot coding. We propose two solutions: (a) decrease w_{ce} increase w_{kl} at the same time; (b) decrease α increase β at the same time; Specifically, (a) aims to transfer more dark knowledge to the student, while (b) aims to make the teacher not overconfident about the augmented samples searched by Stage II. As exhibited in Tab. 9, both methods assist in bridging the gap between the teacher and student to some extent.

What are the characteristics of $\{\theta_m^i\}_{i=1}^{N-N_{nl}}$ and $\{\theta_p^i\}_{i=1}^N$ searched by TST? To answer this question, we choose 8 magnitudes and probabilities from $\{\theta_m^i\}_{i=1}^{N-N_{nl}}$ and $\{\theta_p^i\}_{i=1}^N$ with distinct patterns and plot their variation with iteration in Fig. 3. The full TST visualization of search results is shown in Appendix D. Note that there are 3 teacher-student pairs, i.e., WRN-40-2-WRN-16-2, WRN40-2-WRN-

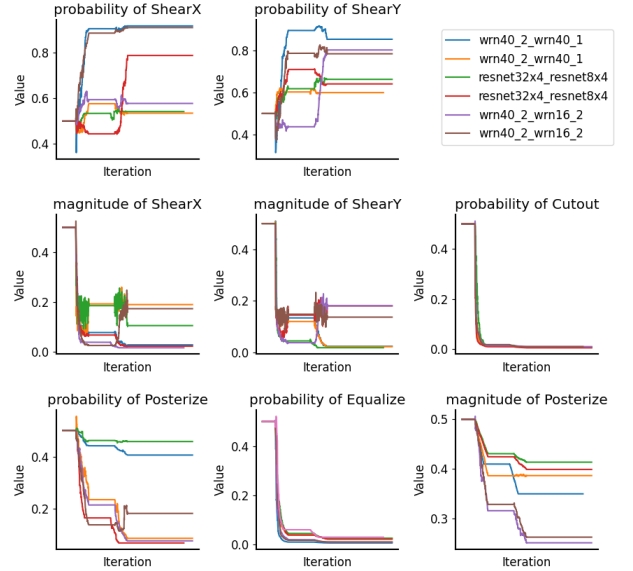


Figure 3: The plot of magnitudes and probabilities variation with iteration under OSD on CIFAR-100. Here we have selected representative sub-policies, including ShearX, ShearY, Cutout, Posterize, and Equalize.

40-1 and ResNet32x4-ResNet8x4 pairs in these figures, and each pair has two change curves. Although the magnitudes and probabilities searched by the different models are various, they have macroscopic similarities. For instance, ShearX and ShearY converge to larger probabilities and smaller magnitudes; sub-policies without learnable magnitudes, such as Equalize and Cutout, converge to minimal probabilities. In fact, such a result is intuitive. For instance, the characteristics of the dataset let the magnitudes and probabilities searched by the data augmentation methods (e.g., PBA and AutoAugment) on one model can also be applied to another one. Besides, each curve in Fig. 3 differs at a microscopic level due to the difference between teacher-student pairs and the stochastic nature of deep learning.

6 Conclusion

In this paper, inspired by realistic teaching scenarios, we design a data-based distillation algorithm called TST. To be specific, TST introduces the priori bias at Stage I that can facilitate convergence and improve distillation performance. Then, it locates augmented samples in Stage II that the teacher is good at while the student is not, and transfers the knowledge of these augmented samples from the teacher to the student through Stage III. Finally, repeat Stage II and Stage III continuously until an excellent student is obtained. In future research, the data-based distillation, which is as competitive as logit-based and feature-based distillation, may deserve the attention of scholars.

References

[1] Sungsoo Ahn, Shell Xu Hu, Andreas Damianou, Neil D Lawrence, and Zhenwen Dai. Variational information distillation for knowledge transfer. In *Computer Vision and Pattern Recognition*, pages 9163–9171, Long Beach, CA, USA, Jun. 2019. IEEE.

[2] Tom Brown, Benjamin Mann, Nick Ryder, Melanie Subbiah, Jared D Kaplan, Prafulla Dhariwal, Arvind Neelakantan, Pranav Shyam, Girish Sastry, Amanda Askell, et al. Language models are few-shot learners. In *Neural Information Processing Systems*, volume 33, pages 1877–1901, Virtual Event, Dec. 2020. NIPS.

[3] Nicholas Carlini and David Wagner. Towards evaluating the robustness of neural networks. In *Security and Privacy*, pages 39–57. IEEE, 2017.

[4] Hanting Chen, Yunhe Wang, Tianyu Guo, Chang Xu, Yiping Deng, Zhenhua Liu, Siwei Ma, Chunjing Xu, Chao Xu, and Wen Gao. Pre-trained image processing transformer. In *Computer Vision and Pattern Recognition*, pages 12299–12310, Virtual Event, Jun. 2021.

[5] Kai Chen, Jiaqi Wang, and Pang et al. MMDetection: Open mmlab detection toolbox and benchmark. *arXiv preprint arXiv:1906.07155*, 2019.

[6] Pengguang Chen, Shu Liu, Hengshuang Zhao, and Jiaya Jia. Distilling knowledge via knowledge review. In *Computer Vision and Pattern Recognition*, pages 5008–5017, Virtual Event, Jun. 2021. IEEE.

[7] Po-Wei Chou, Daniel Maturana, and Sebastian Scherer. Improving stochastic policy gradients in continuous control with deep reinforcement learning using the beta distribution. In *International Conference on Machine Learning*, pages 834–843, Stockholm Sweden, Aug. 2017. PMLR.

[8] Linhang Cai, Yongjun Xu, Chuanguang Yang, Zhulin An. Hierarchical self-supervised augmented knowledge distillation. In *Conference on Association for the Advancement of Artificial Intelligence*, pages 1217–1223, Montreal, Aug. 2021. AAAI.

[9] MM Segmentation Contributors. MM Segmentation: Openmmlab semantic segmentation toolbox and benchmark, 2020.

[10] MM Razor Contributors. Openmmlab model compression toolbox and benchmark, 2021.

[11] Marius Cordts, Mohamed Omran, Sebastian Ramos, Timo Rehfeld, Markus Enzweiler, Rodrigo Benenson, Uwe Franke, Stefan Roth, and Bernt Schiele. The cityscapes dataset for semantic urban scene understanding. In *Computer Vision and Pattern Recognition*, pages 3213–3223, Las Vegas, NV, USA, Jun.-Jul. 2016. IEEE.

[12] Ekin D Cubuk, Barret Zoph, Dandelion Mane, Vijay Vasudevan, and Quoc V Le. Autoaugment: Learning augmentation strategies from data. In *Computer Vision and Pattern Recognition*, pages 113–123, Long Beach, CA, USA, Jun. 2019. IEEE.

[13] Ekin D Cubuk, Barret Zoph, Jonathon Shlens, and Quoc V Le. Randaugment: Practical automated data augmentation with a reduced search space. In *Computer Vision and Pattern Recognition workshops*, pages 702–703, Seattle, WA, USA, Jun. 2020. IEEE.

[14] Tao Dai, Jianrui Cai, Yongbing Zhang, Shu-Tao Xia, and Lei Zhang. Second-order attention network for single image super-resolution. In *Computer Vision and Pattern Recognition*, pages 11057–11066, Long Beach, CA, USA, Jun. 2019. IEEE.

[15] Xing Dai, Zeren Jiang, Zhao Wu, Yiping Bao, Zhicheng Wang, Si Liu, and Erjin Zhou. General instance distillation for object detection. In *Computer Vision and Pattern Recognition*, pages 7842–7851, Virtual Event, Jun. 2021.

[16] Zihang Dai, Zhilin Yang, Yiming Yang, Jaime Carbonell, Quoc Le, and Ruslan Salakhutdinov. Transformer-XL: Attentive language models beyond a fixed-length context. In *Association for Computational Linguistics*, pages 2978–2988, Florence, Italy, Jul. 2019. ACL.

[17] Jacob Devlin, Ming-Wei Chang, Kenton Lee, and Kristina Toutanova. Bert: Pre-training of deep bidirectional transformers for language understanding. *arXiv preprint arXiv:1810.04805*, 2018.

[18] Gongfan Fang, Kanya Mo, Xinchao Wang, Jie Song, Shitao Bei, Haofei Zhang, and Mingli Song. Up to 100x faster data-free knowledge distillation. In *Association for the Advancement of Artificial Intelligence*, number 6, pages 6597–6604, Virtual Event, Feb.-Mar. 2022.

[19] Jonathan Frankle and Michael Carbin. The lottery ticket hypothesis: Finding sparse, trainable neural networks. In *International Conference on Learning Representations*, New Orleans, LA, USA, May 2019.

[20] Ian Goodfellow, Jean Pouget-Abadie, Mehdi Mirza, Bing Xu, David Warde-Farley, Sherjil Ozair, Aaron Courville, and Yoshua Bengio. Generative adversarial networks. *Communications of the ACM*, (11):139–144, 2020.

[21] Kaiming He, Xinlei Chen, Saining Xie, Yanghao Li, Piotr Dollár, and Ross Girshick. Masked autoencoders are scalable vision learners. In *Computer Vision and Pattern Recognition*, pages 16000–16009, New Orleans, LA, USA, Jun. 2022. IEEE.

[22] Byeongho Heo, Jeesoo Kim, Sangdoo Yun, Hyojin Park, Nojun Kwak, and Jin Young Choi. A comprehensive overhaul of feature distillation. In *International Conference on Computer Vision*, pages 1921–1930, Seoul, Korea (South), Oct.-Nov. 2019. IEEE.

[23] Geoffrey Hinton, Oriol Vinyals, Jeff Dean, et al. Distilling the knowledge in a neural network. *arXiv preprint arXiv:1503.02531*, 2(7), 2015.

[24] Jonathan Ho, Ajay Jain, and Pieter Abbeel. Denoising diffusion probabilistic models. In *Neural Information Processing Systems*, pages 6840–6851, Virtual Event, Dec. 2020. NIPS.

[25] Tao Huang, Shan You, Fei Wang, Chen Qian, and Chang Xu. Knowledge distillation from a stronger teacher. In *Neural Information Processing Systems*, New Orleans, LA, USA, Nov.-Dec. 2022. NIPS.

[26] Max Jaderberg, Karen Simonyan, Andrew Zisserman, and koray kavukcuoglu. Spatial transformer networks. In *Neural Information Processing Systems*, volume 28, Montréal, Canada, Dec. 2015. Curran Associates, Inc.

[27] Diederik P Kingma and Max Welling. Auto-encoding variational bayes. *arXiv preprint arXiv:1312.6114*, 2013.

[28] Alex Krizhevsky and Geoffrey Hinton. Learning multiple layers of features from tiny images. *Handbook of Systemic Autoimmune Diseases*, 2009.

[29] Yonggang Li, Guosheng Hu, Yongtao Wang, Timothy M. Hospedales, Neil Martin Robertson, and Yongxing Yang. DADA: differentiable automatic data augmentation. In *European Conference on Computer Vision*, Virtual Event, Aug. 2020. Springer.

[30] Sungbin Lim, Ildoo Kim, Taesup Kim, Chiheon Kim, and Sungwoong Kim. Fast autoaugment. In *Neural Information Processing Systems*, pages 6662–6672, Jan.

[31] Tsung-Yi Lin, Michael Maire, Serge Belongie, James Hays, Pietro Perona, Deva Ramanan, Piotr Dollár, and C Lawrence Zitnick. Microsoft coco: Common objects in context. In *European Conference on Computer Vision*, pages 740–755, Zurich, Switzerland, Sept. 2014. Springer.

[32] Yifan Liu, Ke Chen, Chris Liu, Zengchang Qin, Zhenbo Luo, and Jingdong Wang. Structured knowledge distillation for semantic segmentation. In *Computer Vision and Pattern Recognition*, pages 2604–2613, Long Beach, CA, USA, Jun. 2019. IEEE.

[33] Yifan Liu, Changyong Shu, Jingdong Wang, and Chunhua Shen. Structured knowledge distillation for dense prediction. *IEEE transactions on Pattern Analysis and Machine Intelligence*, 2020.

[34] Ze Liu, Yutong Lin, Yue Cao, Han Hu, Yixuan Wei, Zheng Zhang, Stephen Lin, and Baining Guo. Swin transformer: Hierarchical vision transformer using shifted windows. In *International Conference on Computer Vision*, pages 10012–10022, Virtual Event, Mar. 2021. IEEE.

[35] Aleksander Madry, Aleksandar Makelov, Ludwig Schmidt, Dimitris Tsipras, and Adrian Vladu. Towards deep learning models resistant to adversarial attacks. In *International Conference on Learning Representations*, Vancouver, Canada, Apr.-May 2018. OpenReview.net.

[36] Sébastien Marcel and Yann Rodriguez. Torchvision the machine-vision package of torch. In *ACM international conference on Multimedia*, pages 1485–1488, Firenze, Italy, Oct. 2010. ACM.

[37] Volodymyr Mnih, Koray Kavukcuoglu, David Silver, Alex Graves, Ioannis Antonoglou, Daan Wierstra, and Martin Riedmiller. Playing atari with deep reinforcement learning. *arXiv preprint arXiv:1312.5602*, 2013.

[38] Wonpyo Park, Dongju Kim, Yan Lu, and Minsu Cho. Relational knowledge distillation. In *Conference on Computer Vision and Pattern Recognition*, pages 3967–3976, Long Beach, CA, USA, Jun. 2019. IEEE.

[39] Nikolaos Passalis and Anastasios Tefas. Learning deep representations with probabilistic knowledge transfer. In *European Conference on Computer Vision*, pages 268–284, Munich, Germany, Sept. 2018. Springer.

[40] Hendrik Purwins, Bo Li, Tuomas Virtanen, Jan Schlüter, Shuo-Yiin Chang, and Tara Sainath. Deep learning for audio signal processing. *IEEE Journal of Selected Topics in Signal Processing*, 13(2):206–219, 2019.

[41] Tabish Rashid et al. QMIX: Monotonic value function factorisation for deep multi-agent reinforcement learning. In *International Conference on Machine Learning*, volume 80, pages 4295–4304, Stockholm, SweDen, Jul. 2018. PMLR.

[42] Joseph Redmon and Ali Farhadi. Yolov3: An incremental improvement. *arXiv preprint arXiv:1804.02767*, 2018.

[43] Adriana Romero, Nicolas Ballas, Samira Ebrahimi Kahou, Antoine Chassang, Carlo Gatta, and Yoshua Bengio. Fitnets: Hints for thin deep nets. *arXiv preprint arXiv:1412.6550*, 2014.

[44] Olga Russakovsky, Jia Deng, Hao Su, Jonathan Krause, Sanjeev Satheesh, Sean Ma, Zhiheng Huang, Andrej Karpathy, Aditya Khosla, Michael Bernstein, et al. Imagenet large scale visual recognition challenge. *International journal of computer vision*, 115(3):211–252, 2015.

[45] Changyong Shu, Yifan Liu, Jianfei Gao, Zheng Yan, and Chunhua Shen. Channel-wise knowledge distillation for dense prediction. In *International Conference on Computer Vision*, pages 5311–5320, Montreal, Canada, Oct. 2021. IEEE.

[46] Teppei Suzuki. Teachaugment: Data augmentation optimization using teacher knowledge. In *Computer Vision and Pattern Recognition*, pages 10904–10914, New Orleans, LA, USA, Jun. 2022. IEEE.

[47] Yonglong Tian, Dilip Krishnan, and Phillip Isola. Contrastive representation distillation. In *International Conference on Learning Representations*, Addis Ababa, Ethiopia, Apr. 2020. OpenReview.net.

[48] Frederick Tung and Greg Mori. Similarity-preserving knowledge distillation. In *International Conference on Computer Vision*, pages 1365–1374, Seoul, Korea (South), Oct-Nov. 2019. IEEE.

[49] Yukang Wang, Wei Zhou, Tao Jiang, Xiang Bai, and Yongchao Xu. Intra-class feature variation distillation for semantic segmentation. In *European Conference on Computer Vision*, pages 346–362, Virtual Event, Aug. 2020. Springer.

[50] Zijian Wang, Yadan Luo, Ruihong Qiu, Zi Huang, and Mahsa Baktashmotagh. Learning to diversify for single domain generalization. In *International Conference on Computer Vision*, pages 834–843, Virtual Event, Oct. 2021. IEEE.

[51] Mikołaj Wieczorek, Barbara Rychalska, and Jacek Dabrowski. On the unreasonable effectiveness of centroids in image retrieval. In *International Conference on Neural Information Processing*, pages 212–223, Bali, Indonesia, Dec. 2021. Springer.

[52] Jiaxiang Wu, Cong Leng, Yuhang Wang, Qinghao Hu, and Jian Cheng. Quantized convolutional neural networks for mobile devices. In *Computer Vision and Pattern Recognition*, Las Vegas, NV, USA, Jun. 2016. IEEE.

[53] Zhendong Yang, Zhe Li, Xiaohu Jiang, Yuan Gong, Zehuan Yuan, Danpei Zhao, and Chun Yuan. Focal and global knowledge distillation for detectors. In *Computer Vision and Pattern Recognition*, pages 4643–4652, New Orleans, LA, USA, Jun. 2022. IEEE.

[54] Hongxu Yin, Pavlo Molchanov, Jose M Alvarez, Zhizhong Li, Arun Mallya, Derek Hoiem, Niraj K Jha, and Jan Kautz. Dreaming to distill: Data-free knowledge transfer via deepinversion. In *Computer Vision and Pattern Recognition*, pages 8715–8724, Seattle, WA, USA, Jun. 2020. IEEE.

[55] Sergey Zagoruyko and Nikos Komodakis. Wide residual networks. In *British Machine Vision Conference*, pages 1–15, York, UK, Sept. 2016. BMVA.

[56] Linfeng Zhang and Kaisheng Ma. Improve object detection with feature-based knowledge distillation: Towards accurate and efficient detectors. In *International Conference on Learning Representations*, Vienna, Austria, May 2021. OpenReview.net.

[57] Borui Zhao, Quan Cui, Renjie Song, Yiyu Qiu, and Jiajun Liang. Decoupled knowledge distillation. In *Conference on Computer Vision and Pattern Recognition*, pages 11953–11962, New Orleans, LA, USA, Jun. 2022. IEEE.

[58] Hengshuang Zhao, Jiaya Jia, and Vladlen Koltun. Exploring self-attention for image recognition. In *Computer Vision and Pattern Recognition*, pages 10076–10085, Seattle, WA, USA, Jun. 2020. IEEE.

[59] Hengshuang Zhao, Jianping Shi, Xiaojuan Qi, Xiaogang Wang, and Jiaya Jia. Pyramid scene parsing network. In *Computer Vision and Pattern Recognition*, Honolulu, HI, USA, Jul. 2017. IEEE.

[60] Du Zhixing, Rui Zhang, Ming Chang, Shaoli Liu, Tianshi Chen, Yunji Chen, et al. Distilling object detectors with feature richness. *Neural Information Processing Systems*, 34:5213–5224, Dec. 2021.

[61] Jun-Yan Zhu, Taesung Park, Phillip Isola, and Alexei A. Efros. Unpaired image-to-image translation using cycle-consistent adversarial networks. In *International Conference on Computer Vision*, Venice, Italy, Oct. 2017. IEEE.

A Datasets

CIFAR-100. Dataset CIFAR-100 [28] is the subsets of the tiny image dataset and consists of 60000 images with the size 32×32 . Specifically, the training set contains 50000 images, and the testing set contains 10000 images.

ImageNet-1k. Dataset ImageNet-1k [44], also commonly referred to as ILSVRC 2012, has 1000 classes, and the benchmark is trained using the training set and tested using the validation set. Its training and validation sets contain 1281167 and 50,000 images, respectively.

MS-COCO. Dataset MS-COCO is a large-scale object detection dataset. The benchmark is the same as ImageNet-1k, using the training set for training and the validation set for testing. The training/validation split was changed from 83K/41K to 118K/5K in 2017. Researchers commonly apply the 2017 version for experiments.

Cityscapes. Dataset Cityscapes is a new large-scale dataset for semantic segmentation. It provides 5000 images that have been meticulously annotated, with 2,975 images for training and 500 images for validation, where 30 common classes are provided and 19 classes are used for evaluation and testing. Each image is 2048×1024 in size.

B Hyperparameter Settings

B.1 Basic settings

Classification. For the classification experiments on CIFAR-100, the batch size is 128, the total number of epochs is 240, and the learning rate is initialized to 0.1 and divided by 10 at 150, 180 and 210 epochs. In addition, we employ an SGD optimizer for training and set the weight decay and momentum as 5e-4 and 0.9, respectively. For the classification experiments on ImageNet-1k (ResNet34-ResNet18 pair and ResNet50-MobileNet pair), the total batch size is 512, the total number of epochs is 100, the batch size in every GPU is 128, the number of GPUs is 4 and the learning rate is initialized to 0.1 and divided by 10 at 30, 60 and 90 epochs. Besides, we employ an SGD optimizer for training and set the weight decay and momentum as 1e-4 and 0.9, respectively. For the Swin-Large-Swin-Tiny pair, we follow the setting in [34], except for the batch size and initial learning rate. Specifically, the batch size is 512, the total number of epochs is 300, the batch size in every GPU is 64, the number of GPUs is 8, and the learning rate is initialized to 0.0005 and is decayed by a cosine scheduler. Furthermore, we utilized an Adam optimizer for training and set the weight decay as 5e-2. The reason for halving the batch size is that the GPU memory is sufficient to support the training with the original hyperparameter settings.

Detection. For the detection experiments on MS-COCO, we utilize mmdetection [5] and mmrazor [10] for both training and testing. Following [45; 38], we use the same standard training strategies on the Cascade RCNN-X101-Faster RCNN-R50 and RetinaNet-X101-RetinaNet-R50 pairs. To be specific, the total batch size is 16, the total number of epochs is 24, the batch size in every GPU is 2, the number of GPUs is 8 and the learning rate is divided by 10 at 16 and

22 epochs. The initial learning rate is set as 0.02 and 0.01 on Cascade RCNN-X101-Faster RCNN-R50 and RetinaNet-X101-RetinaNet-R50 pairs, respectively. Besides, the setting on the FCOS-R101-FCOS-R50 pair is following [53]. Compared with the RetinaNet-X101-RetinaNet-R50 pair, the only difference is we apply a warm-up learning rate on the FCOS-R101-FCOS-R50 pair.

Segmentation. For the segmentation experiments on Cityscapes, we apply mmsegmentation [9] and mmrazor [10] for distillation. we follow the setting in [10]. In specific, the total batch size is 16, the total number of iterations is 80000, the batch size in every GPU is 2, the number of GPUs is 8 and the learning rate is 0.01. We make the learning rate decay to 0.9 in each iteration and constrain the minimum learning rate in training to be 1e-4. And we utilized a SGD optimizer for training and set the weight decay and momentum as 5e-4 and 0.9, respectively.

B.2 Advanced Settings

Classification. On CIFAR-100, the loss weight is set as 1 for all comparison results and the temperature of TST (i.e., vanilla KD) is 4. We let f_{DE} update the magnitudes $\{\theta_m^i\}_{i=1}^{N-N_{nl}}$ and probabilities $\{\theta_p^i\}_{i=1}^N$ (i.e., conduct Stage II) at 30 and 90 epochs and continuously train f_{DE} for 1 epoch. Moreover, on ImageNet-1k, the loss weight is set as 1 for all comparison results and the temperature of TST (i.e., vanilla KD) is 1. The magnitudes $\{\theta_m^i\}_{i=1}^{N-N_{nl}}$ and probabilities $\{\theta_p^i\}_{i=1}^N$ are updated at 10 and 20 epochs. Unlike CIFAR-100 training, we train 5 epochs for f_{DE} continuously.

Detection. On MS-COCO, the loss weight is set as 1 for all comparison results and the temperature of TST (i.e., vanilla KD) is 1. We add \mathcal{L}_{KL} and \mathcal{L}_{MSE} to the final predictions of classes and the neck, respectively. On Stage II, we let not only the student classification predictions but also the student box regression be inaccurate. Compare with the student, we make the teacher’s categorical predictions and box regressions as accurate as possible. Furthermore, We make f_{DE} update the magnitudes $\{\theta_m^i\}_{i=1}^{N-N_{nl}}$ and probabilities $\{\theta_p^i\}_{i=1}^N$ at 6 and 12 epochs and continuously train f_{DE} for 1 epoch.

Segmentation. On Cityscapes, we set the loss weight on \mathcal{L}_{KL} between the teacher decode head’s final predictions and the student decode head’s final predictions as 1.5. In addition, we set the loss weight on \mathcal{L}_{KL} between the teacher auxiliary head’s final predictions and the student auxiliary head’s final predictions as 0.5. Also, the temperature of TST (i.e., vanilla KD) is set as 1. Last but not least, the magnitudes $\{\theta_m^i\}_{i=1}^{N-N_{nl}}$ and probabilities $\{\theta_p^i\}_{i=1}^N$ is updated at 7500 and 15000 iterations on the total training. We continuously update $\{\theta_m^i\}_{i=1}^{N-N_{nl}}$ and probabilities $\{\theta_p^i\}_{i=1}^N$ with 1250 iterations.

C Training Process on TST

In this section, we show the full training process of TST in Algorithm 1. For the sake of simplicity, we do not categorize the different sub-policies here and consistently consider that they are all learnable. Moreover, for the object detection task, Eq. 1 in Algorithm1 can be replaced with other forms, e.g., $\mathcal{L}_{mimic} + \mathcal{L}_{KL} + \mathcal{L}_{CE}$.

Algorithm 1 Training procedure of TST

Input: A student f_S with the parameter θ_S , a teacher model f_T with the parameter θ_T , a data augmentation encoder set $\{f_E^i\}_{i=1}^N$ with the parameter set $\{\theta_E^i\}_{i=1}^N$, a set of the priori manual data-augmentation mappings $\{f_A^i\}_{i=1}^N$, the parameter of probabilities θ_p , the parameter of magnitudes θ_m , dataset \mathcal{X} , the probabilistic transformation function of the ground truth label p , the number of iterations required for the priori manual data augmentation fitting n_{fitting} , the number of iterations required for a encoder training phase n_{encoder} , the number of iterations required for a student training phase n_{student} , the iterative position set for probability and magnitude learning \mathbb{I} , the learning rate η_{θ_S} and η_{θ_E} .

1: Random initialization parameter $\{\theta_E^i\}_{i=1}^N$.

2: **for** $i = 1, \dots, N$ **do**

3: **for** $j = 0, \dots, n_{\text{fitting}}$ **do**

4: Randomly sample a mini-batch, $\{x^k\}_{k=1}^B \sim \mathcal{X}$.

5: Randomly sample the magnitude m .

6: $\{\mathbf{y}_E^{i,k}\}_{k=1}^B = \{f_E^i(x^k, m)\}_{k=1}^B$.

7: $\{\mathbf{y}_A^{i,k}\}_{k=1}^B = \{f_A^i(x^k, m)\}_{k=1}^B$.

8: Compute loss for the data augmentation encoder,

9: $\mathcal{L}_{\text{encoder}}^i = \sum_{k=1}^B \|\mathbf{y}_E^{i,k} - \mathbf{y}_A^{i,k}\|_2$.

9: Update θ_E^i by the gradient ascent,

9: $\theta_E^i \leftarrow \theta_E^i - \eta_{\theta_E} \partial \mathcal{L}_{\text{encoder}}^i / \partial \theta_E^i$.

10: **end for**

11: **end for**

12: Random initialization parameter the parameter of probabilities θ_p and the parameter of magnitudes θ_m .

13: **for** $i = 0, \dots, n_{\text{student}}$ **do**

14: **if** $i \in \mathbb{I}$ **then**

15: **for** $j = 0, \dots, n_{\text{encoder}}$ **do**

16: Randomly sample a mini-batch, $\{x^k\}_{k=1}^B \sim \mathcal{X}$.

17: Calculate new samples $\{\hat{x}^k\}_{k=1}^B$ using Eq. 5.

18: Compute loss for probabilities and magnitudes,

19: $\mathcal{L}_{\text{TST}} = \sum_{k=1}^B (-\log(p(f_S(\hat{x}^k))) - \log(1 - p(f_T(\hat{x}^k))))$

19: Update ϕ by the gradient ascent, $\theta_p, \theta_m \leftarrow \theta_p - \eta_\phi \partial \mathcal{L}_{\text{TST}} / \partial \theta_p, \theta_m - \eta_\phi \partial \mathcal{L}_{\text{TST}} / \partial \theta_m$

20: **end for**

21: **end if**

22: Randomly sample a mini-batch, $\{x^b\}_b^B \sim \mathcal{X}$

23: Calculate new samples $\{\hat{x}^k\}_{k=1}^{2B}$ by Eq. 5 and the concatenation operator.

24: Compute loss \mathcal{L}_S for the student by Eq. 1.

25: Update θ_S by the gradient descent,

25: $\theta_S \leftarrow \theta_S - \eta_{\theta_S} \partial \mathcal{L}_S / \partial \theta_S$

26: **end for**

D Supplementary Details

Details about f_{DE} in object detection tasks. Generally, a target object, after affine transformation and accumulation according to Eq. 5, generates multiple target objects, leading to ambiguity. Thus, we design a method to replace the weighted summation of the difference between the affine transform result and the original image. To be specific, we sum all affine transformation matrices generated from f_{STN} for obtaining only one new target affine transformation matrix \hat{A} . And f_{DE} simply learns \hat{A} that satisfies the objective that TST search. In here, we define two hyperparameters N_a and N_c (s.t., $N_a + N_c = N_{nl}$) refer to the number of learnable affine transformations and learnable color transformations, respectively. Due to all unlearnable transformations are color transformations, we can disregard them. First, for a set of affine meta-encoders $\{f_{STN}^{Z^i}\}_{i=1}^{N_a}$ (s.t., $N_a \leq N_A$)², we can define the set of affine transformation matrices generated by this set as $\{A^{Z^i}\}_{i=1}^{N_a}$. Then, the final matrix \hat{A} generated by f_{DE} can be formulated as:

$$\begin{aligned} A_E^i &= \theta_p^{Z^i} \odot A^{Z^i} - \theta_p^{Z^i} \odot I, \text{ s.t. } Z^i \leq N_a \\ \hat{A} &= I + \sum_{i=1}^{N_a} A_E^i, \end{aligned} \quad (8)$$

where I refers to a matrix $\sim \mathbb{R}^{2 \times 3}$ where only the values on the diagonal are 1 and the rest are 0. After that, we derive \hat{x}_a by the operator Affine.

$$\hat{x}_a = \text{Affine}(\hat{A}, x) \quad (9)$$

Now, we need to apply the remaining meta-encoders to complete the transform of \hat{x}_a . As a result, the corresponding computational form is shown in Eq. 10.

$$\begin{aligned} x_E^i &= \begin{cases} \theta_p^{Z^i} \odot f_E(\hat{x}_a, \theta_m^{Z^i}) - \theta_p^{Z^i} \odot \hat{x}_a, & N_a < Z^i \leq N_{nl} \\ \theta_p^{Z^i} \odot f_E(\hat{x}_a) - \theta_p^{Z^i} \odot \hat{x}_a, & Z^i > N_{nl} \end{cases} \\ \hat{x} &= \hat{x}_a + \sum_{i=N_a+1}^{N_A} x_E^i, \end{aligned} \quad (10)$$

Finally, we obtain \hat{x} , which is a part of the input to f_T and f_S . In particular, \hat{x} in Eq. 5 and Eq. 10 have the same meaning.

Full probability and magnitude visualization. Due to space constraints in the main paper, we only show 8 sub-policies' magnitudes and probabilities searched by TST. So, we illustrate the magnitudes and probabilities of all sub-policies in Fig. 4 (i.e., 11 magnitudes and 14 probabilities).

Proof that $-\mathcal{L}_{CE}(x, y)$ is a non-convex function and $\mathcal{L}_{CE}(1-x, y)$ is a convex function. In $-\mathcal{L}_{CE}(x, y)$ and $\mathcal{L}_{CE}(1-x, y)$, x and y are two vectors whose lengths are the number of categories. Since y is one-hot encoding, this function can be written as $\log(x_t)$, where x_t is the predicted value in x corresponding to the target label. In particular, $0 \leq x_t \leq 1$ due to the presence of the normalization function (i.e., softmax). As the definition of a convex function, we

²Here, for simplicity, we let the first N_a of N_A actual applied meta-encoders all be f_{STN} .

need to prove the following equation (note that deep learning is stochastic gradient descent for parameter updating, so the convex function declared here is downward convex):

$$\log(a+b) \leq \log(a) + \log(b), \quad \text{s.t. } 0 \leq a \leq b \leq 1. \quad (11)$$

Obviously, $a+b \geq 2\sqrt{ab} \geq ab$, so Eq. 11 does not hold and $-\mathcal{L}_{CE}(x, y)$ is a non-convex function. Similarly, for $\mathcal{L}_{CE}(1-x, y)$, we can infer that it is a convex function by Eq. 12 since $ab \leq 1$ is a known condition..

$$\begin{aligned} -\log(2-a-b) &\leq -\log(1-a) - \log(1-b), \\ \text{s.t. } 0 \leq a \leq b \leq 1, \\ \approx & \frac{1}{2-a-b} \leq \frac{1}{(1-a)(1-b)}, \\ \approx & ab \leq 1, \end{aligned} \quad (12)$$

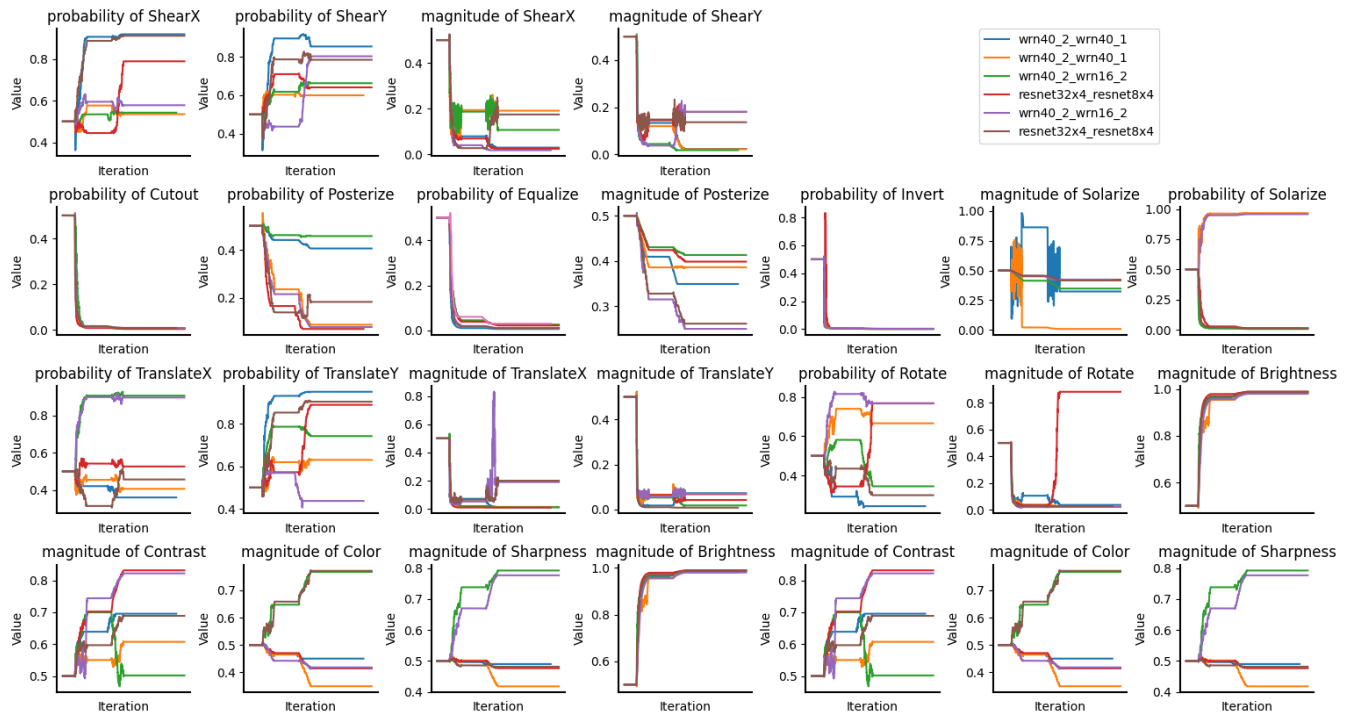


Figure 4: The plot of magnitudes and probabilities variation with iteration under OSD on CIFAR-100. Here we visualize all sub-policies mentioned in this paper.